Available online at www.sciencedirect.com

ScienceDirect

journal homepage: www.elsevier.com/locate/he

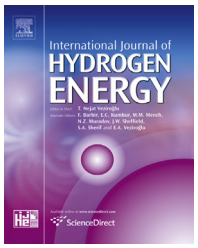

Mechanism of the sonochemical production of hydrogen

Slimane Merouani [a,b,*], *Oualid Hamdaoui* [a], *Yacine Rezgui* [c], *Miloud Guemini* [c]

[a] *Laboratory of Environmental Engineering, Department of Process Engineering, Faculty of Engineering, Badji Mokhtar – Annaba University, P.O. Box 12, 23000 Annaba, Algeria*

[b] *Department of Chemical Engineering, Faculty of Pharmaceutical Engineering Process, University of Constantine 3, 25000 Constantine, Algeria*

[c] *Laboratory of Applied Chemistry and Materials Technology, University of Oum El-Bouaghi, P.O. Box 358, 04000 Oum El Bouaghi, Algeria*

ARTICLE INFO

Article history:
Received 28 December 2014
Received in revised form
23 January 2015
Accepted 27 January 2015
Available online 21 February 2015

Keywords:
Water sonolysis
Hydrogen production
Acoustic cavitation
Kinetics mechanism
Computer simulations

ABSTRACT

It has been long recognized that propagation of an ultrasonic wave in water results in hydrogen production. The chemical effects of ultrasound (sonochemistry) originate from acoustic cavitation, that is, the formation, growth and implosive collapse of microscopic bubbles in liquid irradiated by ultrasound wave. Enormous temperatures and pressures are generated within the bubbles at the collapse, making each bubble as a microreactor within which typical flame reactions occur. The combustion in the cavitation bubbles yield species such as •OH, H•, O, HO_2• and others. Although H_2 is the most molecular product of water sonolysis, the mechanism of its production is until now not understood and the most reported suggestions are controversial. In this paper, a comprehensive numerical work was carried out, for the first time, to explain the mechanism of ultrasound induced generation of H_2 in water. Computer simulations of chemical reactions occurring inside a bubble oscillating in water irradiated by an ultrasonic wave have been performed for different conditions. A kinetics mechanism of 25 reversible chemical reactions was proposed for studying the internal bubble-chemistry. The numerical simulations have evidenced the formation of H_2 as well as other products such as O_2, H_2O_2, •OH, H•, HO_2• and O in the bubble during implosion. In all cases, H_2 was the main product formed in the bubbles at appreciable amount. Basing on the simulation results and using material balance for hydrogen in the gas and liquid phases, the production rate of H_2 in each phase has been quantified. The conclusion was that the main source of H_2 production during water sonolysis is the gas phase of the bubbles through the reaction $H^{\bullet} + {}^{\bullet}OH \leftrightarrow H_2 + O$.

Copyright © 2015, Hydrogen Energy Publications, LLC. Published by Elsevier Ltd. All rights reserved.

* *Corresponding author*. Department of Chemical Engineering, Faculty of Pharmaceutical Engineering Process, University of Constantine 3, 25000 Constantine, Algeria. Tel./fax: +213 (0) 38876560.
E-mail addresses: s.merouani@yahoo.fr, s.merouani03@gmail.com (S. Merouani).

http://dx.doi.org/10.1016/j.ijhydene.2015.01.150

0360-3199/Copyright © 2015, Hydrogen Energy Publications, LLC. Published by Elsevier Ltd. All rights reserved.

Introduction

Approximately 80% of the present world energy demand comes from fossil fuels [1]. Unlike fossil fuels, hydrogen gas (H_2) burns cleanly without emitting any environmental pollutants [2]. In addition, H_2 is also abundantly available in the universe and processes the highest energy content per unit of weight (i.e. 120.7 kJ/g) compared to any of the known fuels [1]. H_2 is considered to be the energy carrier of the future [3] and could have an important role in reducing environmental emissions. Several techniques have been used in the past for producing hydrogen. Steam methane reforming is the most widely used method for producing it [1,4]. Alternative ways could be used to generate H_2 such as ethanol gasification [5], water electrolysis [4,6], biological photosynthesis [7,8] and photocatalysis [9–11]. More recently, sonolysis of water have been successfully used for producing hydrogen [12–14]. Moreover, ultrasonication assisted hydrogen production from catalysis [15], photocatalysis [16–18], digestion sludge [19–21] and anaerobic fermentation of wastewater [22] have proven their improvement potential compared to each isolated technique (without ultrasound).

Since 1962, it has been recognized that propagation of an ultrasonic wave in aqueous solution (simply known as sonolysis) containing a solute can results in an oxidation process, which is called sonochemistry [23]. Besides this process, it was well established that H_2O_2 and H_2 are the main products of pure water sonolysis and the ratio of H_2 to H_2O_2 production is ~1.25 [13,14,24]. The generation of H_2 by water sonolysis does not arise from the direct interaction between acoustic wave and water but it produces upon acoustic cavitation, that is, the formation, growth and violently collapse of microscopic bubbles (filled with water vapor and dissolved gases) in a liquid medium irradiated by an ultrasonic wave (Fig. 1) [25]. The rapid collapse of these microbubbles is nearly adiabatic, making each bubble as a powered microreactor inside which temperature of several thousands of Kelvin and pressure of several hundreds of atmospheres are reached [26]. Under these enormous conditions, high temperature combustion-chemistry occurs in the bubble [27]. In fact, the trapped molecules in the bubble (water vapor, gases and vaporized solutes) can be brought to an excited-state and dissociate. As results, reactive species such as •OH, HO_2•, H•, O and H_2O_2 are created from H_2O and O_2 dissociation and their associate reactions in the bubble [28]. These chemical products may diffuse out of the bubble and dissolve in the surrounding liquid [29]. One of the most products of water sonolysis is hydrogen (H_2). It may be formed at rate of 10–15 μM min^{-1} [13,14,24], which is much higher than that obtained by photocatalysis (~0.035 μM min^{-1} [16]).

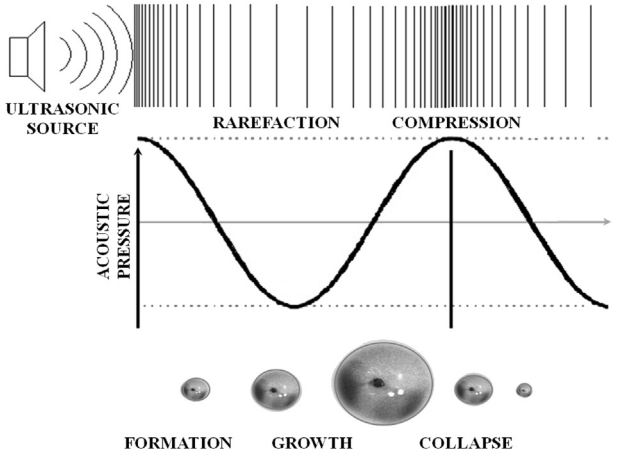

Fig. 1 – Dynamics of acoustic cavitation bubble.

The mechanism of H_2 production from water sonolysis is until now under discussion. A number of researches [24,30,31] postulated that the major part of H_2 is produced in the gas phase of the bubble and diffused to the solution whereas others [32,33] indicated that H_2 is formed only at the liquid shell of the bubble by the recombination of hydrogen radicals diffused from the bubble ($H^{\bullet}+H^{\bullet}\leftrightarrow H_2$). However, to the best of our knowledge, the mechanism of hydrogen production from water sonolysis is until now not understood. The present work is a contribution to the study of the mechanism of hydrogen generation during water sonolysis. A series of numerical simulations of chemical reactions occurring in the interior of an argon bubble oscillating in liquid water irradiated by an ultrasonic wave have been performed for various conditions. A kinetics mechanism of 25 reversible chemical reactions was postulated for studying the internal bubble-chemistry. On the basis of the simulation results, material balance for hydrogen in the gas and liquid phases has been carried out to evaluate the importance of each of the controversial reported suggestions and then determine the mechanism of H_2 generation during water sonolysis.

Model and computational methods

The theoretical model used in the present numerical simulations have been described in our previous works [34–36]. It combines the dynamic of single bubble in acoustic field with chemical kinetics consisting of series of chemical reactions occurring in the bubble at the collapse phase. The following is a brief description of the model.

Bubble dynamics model

A gas and vapor filled spherical bubble isolated in water oscillates under the action of a sinusoidal sound wave. The temperature and pressure in the bubble are assumed to be partially uniform and the gas content of the bubble behaves as an ideal gas [37]. The radial dynamics of the bubble is described by the Keller equation that includes first order terms in the Mach number $M=\dot{R}/c$ [38,39]:

$$\left(1-\frac{\dot{R}}{c}\right)R\ddot{R}+\frac{3}{2}\left(1-\frac{\dot{R}}{3c}\right)\dot{R}^2=\frac{1}{\rho_L}\left(1+\frac{\dot{R}}{c}+\frac{R}{c}\frac{d}{dt}\right)\left[p-p_\infty-\frac{2\sigma}{R}-4\mu\frac{\dot{R}}{R}+P_A\sin(2\pi ft)\right] \quad (1)$$

in this equation dots denote time derivatives (d/dt), R is the radius of the bubble, c is the speed of sound in the liquid, ρ_L is

the density of the liquid, σ is the surface tension, μ is the liquid viscosity, p is the pressure inside the bubble, p_∞ is the ambient static pressure, P_A is the acoustic amplitude and f is the sound frequency. The acoustic amplitude P_A is correlated with the acoustic intensity I_a, or power per unit area, as $P_A = (2I_a\rho_L c)^{1/2}$ [29].

The expansion of the bubble is assumed as isothermal and its total compression is considered as adiabatic [40]. These assumptions, which are widely accepted since the lifetime of an oscillation at high frequency is relatively short with a very rapidly occurring collapse event, were pointed out by Yasui et al. [41] using a more detailed model. We also assume that the vapor pressure in the bubble remains constant during the bubble expansion phase and there is no gas diffusion during expansion and no mass and heat transfer of any kind during collapse. Storey and Szeri [42] demonstrated that the inclusion of mass transfer on the bubble dynamics has practically no effect on the maximum bubble temperature attained in the bubble at the collapse when the compression ratio of the bubble (R_{max}/R_{min}) is less than 20 (R_{max} is the maximum radius of the bubble and R_{min} is the minimum bubble radius at the collapse). This level of R_{max}/R_{min} was never attained in the present numerical study. Therefore, in order to reduce computational parameters, the current model takes, as input, initial bubble vapor content and neglects mass and heat transfer during bubble expansion and collapse.

Based on the above assumptions, the pressure and temperature inside the bubble at any instant during the collapse phase can be calculated from the bubble size as

$$p = \left[P_v + P_{g_0}\left(\frac{R_0}{R_{max}}\right)^3\right]\left(\frac{R_{max}}{R}\right)^{3\gamma} \tag{2}$$

$$T = T_\infty\left(\frac{R_{max}}{R}\right)^{3(\gamma-1)} \tag{3}$$

where P_v is the vapor pressure, $P_{g0} = p_\infty + (2\sigma/R_0) - P_v$ is the gas pressure in the bubble at its ambient state ($R = R_0$), R_0 is the ambient bubble radius, T_∞ is the bulk liquid temperature and γ is the ratio of specific heats capacities (c_p/c_v) of the gas/vapor mixture. The maximum internal temperature (T_{max}) and pressure (p_{max}) in the bubble are reached at the end of the bubble collapse and they are approximated by:

$$T_{max} = T_\infty\left(\frac{R_{max}}{R_{min}}\right)^{3(\gamma-1)} \tag{4}$$

$$p_{max} = \left[P_v + P_{g_0}\left(\frac{R_0}{R_{max}}\right)^3\right]\left(\frac{R_{max}}{R_{min}}\right)^{3\gamma} \tag{5}$$

It is important to notice here that the assumption of spatial uniform pressure and temperature inside the bubble is valid as long as inertia effects are negligible and the velocity of the bubble wall is below the speed of sound in the vapor/gas mixture. This assumption was justified in detail in the paper published by Kamath et al. [43]. In addition, Yasui et al. [41] and Fujikawa and Akamatzu [44] pointed out in their complete models which include heat transfer that the bubble temperature and pressure are roughly uniform except at a very thin layer, called thermal boundary, near the bubble wall.

Chemical kinetics model

A kinetics mechanism consisting in 19 chemical reactions and their backwards reactions (Table 1) is taken into account involving Ar, O_2, H_2O, •OH, H•, O, HO_2•, H_2 and H_2O_2 species. The scheme in Table 1 has been partially validated from hydrogen flame studies [45] as well as shock-tube and reactor-type experiments [46].

Rate expressions for the chemical reactions consider elementary reversible reactions involving K chemical species, which can be represented in the general form as

$$\sum_{k=1}^{K} \upsilon'_{ki} X_k \leftrightarrow \sum_{k=1}^{K} \upsilon'_{ki} X_k \tag{6}$$

in which υ_{ki} in the stoichiometric coefficients of the ith reaction and X_k is the chemical symbol for the kth species. The superscript $'$ indicates forward stoichiometric coefficients, while $''$ indicates reverse stoichiometric coefficients. The production rate $\dot{w}_k$ of the kth species can be written as a summation of the rate of the variables for all reactions involving the kth species:

$$\dot{w}_k = \frac{1}{V}\frac{dn_k}{dt} = \sum_{i=1}^{I}\left(\upsilon'_{ki} - \upsilon'_{ki}\right) r_i \quad k = 1, \ldots K \tag{7}$$

where n_k is the number of moles of the kth species and V is the volume of the bubble.

The rate r_i for the ith reaction is given by the difference of the forward and reverse rates as

$$r_i = k_{f_i}\prod_{k=1}^{K}[X_k]^{\upsilon'_{ki}} - k_{r_i}\prod_{k=1}^{K}[X_k]^{\upsilon'_{ki}} \tag{8}$$

where $[X_k]$ is the molar concentration of the kth species and k_{fi} and k_{ri} are the forward and reverse rate constants of the ith reaction, respectively. The forward and reverse rate constants for the ith reactions are assumed to have the following Arrhenius temperature dependence:

$$k_{fi} = A_{fi}T^{b_{fi}}\exp\left(-\frac{E_{a_{fi}}}{R_g T}\right) \tag{9}$$

$$k_{ri} = A_{ri}T^{b_{ri}}\exp\left(-\frac{E_{a_{ri}}}{R_g T}\right) \tag{10}$$

where R_g is the universal gas constant, A_{fi} (A_{ri}) is the pre-exponential factor, b_{fi} (b_{ri}) is the temperature exponent and E_{fi} (E_{ri}) is the activation energy. Arrhenius parameters of each chemical reaction are listed in Table 1.

In some reactions of Table 1, a third body is required for the reaction to process. When a third body is needed, the reaction rate r_i of the ith reaction should be rewritten as

$$r_i = \left(\sum_{k=1}^{K}\alpha_{ki}[X_k]\right)k_{fi}\prod_{k=1}^{K}[X_k]^{\upsilon'_{ki}} - k_{ri}\prod_{k=1}^{K}[X_k]^{\upsilon'_{ki}} \tag{11}$$

α_{ki} is the third body efficiency factor of species k in the ith reaction.

Table 1 – Scheme of the possible chemical reactions inside a collapsing argon bubble [28,29,34,37,39,40]. M is the third body. Subscript "f" denotes the forward reaction and "r" denotes the reverse reaction. A is in ($cm^3\ mol^{-1}\ s^{-1}$) for two body reaction [($cm^6\ mol^{-2}\ s^{-1}$) for a three body reaction], and E_a is in ($cal\ mol^{-1}$).

Reaction	A_f	b_f	E_{af}	A_r	b_r	E_{ar}
R1. $H_2O + M \leftrightarrow H^\bullet + {}^\bullet OH + M$	1.912×1023	−1.83	1.185×10^5	2.200×1022	−2.00	0.00
R2. $^\bullet OH + M \leftrightarrow O + H^\bullet + M$	9.880×1017	−0.74	1.021×10^5	4.714×1018	−1.00	0.00
R3. $O + O + M \leftrightarrow O_2 + M$	6.165×1015	−0.50	0.00	4.515×1017	−0.64	1.189×10^5
R4. $H^\bullet + O_2 \leftrightarrow O + {}^\bullet OH$	1.915×1014	0.00	1.644×10^4	5.481×1011	0.39	-2.93×10^2
R5. $H^\bullet + O_2 + M \leftrightarrow HO_2^\bullet + M$	1.475×1012	0.60	0.00	3.090×1012	0.53	4.887×10^4
R6. $O + H_2O \leftrightarrow {}^\bullet OH + {}^\bullet OH$	2.970×106	2.02	1.340×10^4	1.465×105	2.11	-2.904×10^3
R7. $HO_2^\bullet + H^\bullet \leftrightarrow H_2 + O_2$	1.660×1013	0.00	8.230×10^2	3.164×1012	0.35	5.551×10^4
R8. $HO_2^\bullet + H^\bullet \leftrightarrow {}^\bullet OH + {}^\bullet OH$	7.079×1013	0.00	2.950×10^2	2.027×1010	0.72	3.684×10^4
R9. $HO_2^\bullet + O \leftrightarrow {}^\bullet OH + O_2$	3.250×1013	0.00	0.00	3.252×1012	0.33	5.328×10^4
R10. $HO_2^\cdot + {}^\bullet OH \leftrightarrow H_2O + O_2$	2.890×1013	0.00	-4.970×10^2	5.861×1013	0.24	6.908×10^4
R11. $H_2 + M \leftrightarrow H^\bullet + H^\bullet + M$	4.577×1019	−1.40	1.044×10^5	1.146×1020	−1.68	8.200×10^2
R12. $O + H_2 \leftrightarrow H^\bullet + {}^\bullet OH$	3.820×1012	0.00	7.948×10^3	2.667×104	2.65	4.880×10^3
R13. $^\bullet OH + H_2 \leftrightarrow H^\bullet + H_2O$	2.160×108	1.52	3.450×10^3	2.298×109	1.40	1.832×10^4
R14. $H_2O_2 + O_2 \leftrightarrow HO_2^\cdot + HO_2^\cdot$	4.634×1016	−0.35	5.067×10^4	4.200×1014	0.00	1.198×10^4
R15. $H_2O_2 + M \leftrightarrow {}^\bullet OH + {}^\bullet OH + M$	2.951×1014	0.00	4.843×10^4	1.00×1014	−0.37	0.00
R16. $H_2O_2 + H^\bullet \leftrightarrow H_2O + {}^\bullet OH$	2.410×1013	0.00	3.970×10^3	1.269×108	1.31	7.141×10^4
R17. $H_2O_2 + H^\bullet \leftrightarrow H_2 + HO_2^\cdot$	6.025×1013	0.00	7.950×10^3	1.041×1011	0.70	2.395×10^4
R18. $H_2O_2 + O \leftrightarrow {}^\bullet OH + HO_2^\cdot$	9.550×106	2.00	3.970×10^3	8.660×103	2.68	1.856×10^4
R19. $H_2O_2 + {}^\bullet OH \leftrightarrow H_2O + HO_2^\cdot$	1.000×1012	0.00	0.00	1.838×1010	0.59	3.089×10^4

Third body efficiency factors R1: $\alpha_{H_2} = 0.73$, $\alpha_{H_2O} = 12$, $\alpha_{Ar} = 0.38$; R2: $\alpha_{H_2} = 2.5$, $\alpha_{H_2O} = 12$, $\alpha_{Ar} = 0.83$. R2: $\alpha_{H_2} = 2.5$, $\alpha_{H_2O} = 12$, $\alpha_{Ar} = 0.75$; R5: $\alpha_{H_2} = 1.3$, $\alpha_{H_2O} = 14$, $\alpha_{Ar} = 0.67$. R11: $\alpha_{H_2} = 2.5$, $\alpha_{H_2O} = 12$; R15: $\alpha_{H_2} = 2.5$, $\alpha_{H_2O} = 12$, $\alpha_{Ar} = 0.64$.

Procedure of the numerical simulation

The Keller–Miksis equation (Eq. (1)), describing the dynamic of the bubble, is a non-linear second-order differential equation which requires an approximate numerical method for solution. Eq. (1) can be reduced to a system of two differential first-order equations

$$\frac{dR}{dt} = \dot{R} \tag{12}$$

$$\frac{d\dot{R}}{dt} = \frac{\frac{1}{\rho_L}\left(1+\frac{\dot{R}}{c}+\frac{R}{c}\frac{d}{dt}\right)\left[p - p_\infty - \frac{2\sigma}{R} - 4\mu\frac{\dot{R}}{R} + P_A \sin\left(2\pi f t\right)\right] - \frac{3}{2}\left(1-\frac{\dot{R}}{3c}\right)\dot{R}^2}{\left(1-\frac{\dot{R}}{c}\right)R} \tag{13}$$

The simulation of the chemical reactions in the bubble starts at the beginning of the adiabatic phase (at time corresponding to $R = R_{max}$). The application of Eq. (7) for all species (9 species) involved in the scheme of Table 1 gives a system of nine ordinary differential equations. For example, according to Table 1, the application of Eq. (7) to the H_2O species gives:

$$\begin{aligned} w_k &= \frac{1}{V}\frac{dn_{H_2O}}{dt} \\ &= -\left\{k_{f1}[H_2O][M] - k_{r1}[H^\bullet][{}^\bullet OH][M]\right\} - \left\{k_{f3}[H_2O][O] - k_{r3}[{}^\bullet OH]^2\right\} \\ &\quad - \left\{k_{f6}[H_2O][H] - k_{r6}[H_2]\left[{}^\bullet OH\right]\right\} - \left\{k_{f9}[H_2O]\left[HO_2^\cdot\right]\right. \\ &\quad \left. - k_{r9}[H_2O_2]\left[{}^\bullet OH\right]\right\} \end{aligned} \tag{14}$$

when V is the volume of the bubble and n_{H_2O} is the number of moles of H_2O.

Using the ideal-gas law $PV = n_tRT$, Eq. (14) can be rewritten as

$$\frac{dn_{H_2O}}{dt} = -\frac{ntRT}{p}\left\langle \begin{array}{l} \left\{k_{f1}[H_2O][M] - k_{r1}[H^\bullet][{}^\bullet OH][M]\right\} + \left\{k_{f3}[H_2O][O] - k_{r3}[{}^\bullet OH]^2\right\} - \\ \left\{k_{f6}[H_2O][H] - k_{r6}[H_2]\left[{}^\bullet OH\right]\right\} + \left\{k_{f9}[H_2O]\left[HO_2^\cdot\right] - k_{r9}[H_2O_2]\left[{}^\bullet OH\right]\right\} \end{array} \right\rangle \tag{15}$$

The system of Eqs. (12) and (13) was solved by the fourth-order Runge–Kutta method using the following initial conditions:

$$t = 0,\ R = R_0 \quad \text{and} \quad \dot{R} = 0$$

The physical properties used for numerical calculations are given for water at 20 °C as $\rho_L = 998.12\ kg\ m^{-3}$, $\sigma = 72.45 \times 10^{-3}\ N\ m^{-1}$, $\mu = 10^{-3}\ kg\ s^{-1}\ m^{-1}$ and $c = 1482\ m\ s^{-1}$.

where n_t is number of mole of all species present in the bubble.

The input parameters for solving the system of the ordinary differential equations obtained by Eq. (7) are the composition of the bubble on water vapor and argon at time corresponding to $R = R_{max}$, the temperature and pressure profiles in the bubble during adiabatic phase and the collapse time. These parameters are obtained by solving the dynamic equation (Eq. (1)). As the bubble temperature increases during the adiabatic phase, the reaction system evolves and radicals

start to form by thermal dissociation of H_2O in the bubble. Thus, the composition of the bubble on all species expected to be present was determined at any temperature during the collapse period by solving the system of the ordinary differential equations obtained by Eq. (7). The system of the ordinary differential equations was solved by the finite difference method. The computer simulation of the reactions system was stopped after the end of the bubble collapse.

Results and discussion

The range of ultrasound frequency commonly used in sonochemistry is from 20 kHz to ~1 MHz. However, based on some experimental results, the optimum ultrasonic frequency for sonochemistry has been reported to be around 355 kHz with regard to the rate of oxidants production by bubbles [47–50]. On the other hand, the ultrasonic frequency at 20 kHz has been mostly used for sonochemistry. Thus, the present numerical simulations have been performed for 20 and 355 kHz. In these conditions, the mean ambient radius (R_0) of active bubbles are determined experimentally as 7.5 μm at 20 kHz [51,52] and 3.2 μm at 355 kHz [53]. The active bubbles are those bubbles that collapse violently and are capable for producing sonochemistry. Furthermore, as hydrogen was quantified in the most cases during the sonolysis of water saturated with argon [13,14,24], the numerical simulations have been performed for an argon bubble.

In Figs. 2 and 3, the results of the numerical simulations have been shown at 20 and 355 kHz. In Figs. 2(a) and 3(a), the liquid pressure applied on the bubble, which is the sum of the acoustic pressure and the static pressure, have been shown for one acoustic period (50 μs at 20 kHz and 2.8 μm at 355 kHz). In Figs. 2(b) and 3(b), the bubble radius has been shown as function of time for one acoustic cycle. It was seen that the bubble initially expands during the rarefaction phase of ultrasound wave, reaching a resonance size ($15.7R_0$ at 20 kHz and $3R_0$ at 355 kHz) at around the end of the rarefaction cycle and then violently collapses to a minimum size (~$0.7R_0$ at 20 kHz and ~$0.5R_0$ μm at 355 kHz) during the compression phase of ultrasound. The bubble then continuous with an equilibrium size before a successive expansion period. In Figs. 2(c) and 3(c), the bubble wall speeds have been shown as function of time. It was seen that the speeds of the bubble wall increased drastically during the final stage of the implosion and attained values of 346 and 71.6 m s^{-1} at respectively 20 and 355 kHz and then decreased very soon. These high speeds of implosion generate stronger collapses, which yielded enormous conditions inside the bubbles. Indeed, the bubble internal pressure may increase up to 4090 and 238 atm at the end of the bubble collapse at respectively 20 and 355 kHz, as can be seen in Figs. 2(d) and 3(d). Correspondingly, the temperature inside a bubble attained 6060 and 5300 K at the end of the bubble collapse at respectively 20 and 355 kHz. Such extreme conditions produced inside the bubble providing a unique environment where high-energy chemical reactions occur as can be seen in Fig. 4, which is an enlargement view of the chemical reactions occurring in the bubble at the final stage of the bubble collapse.

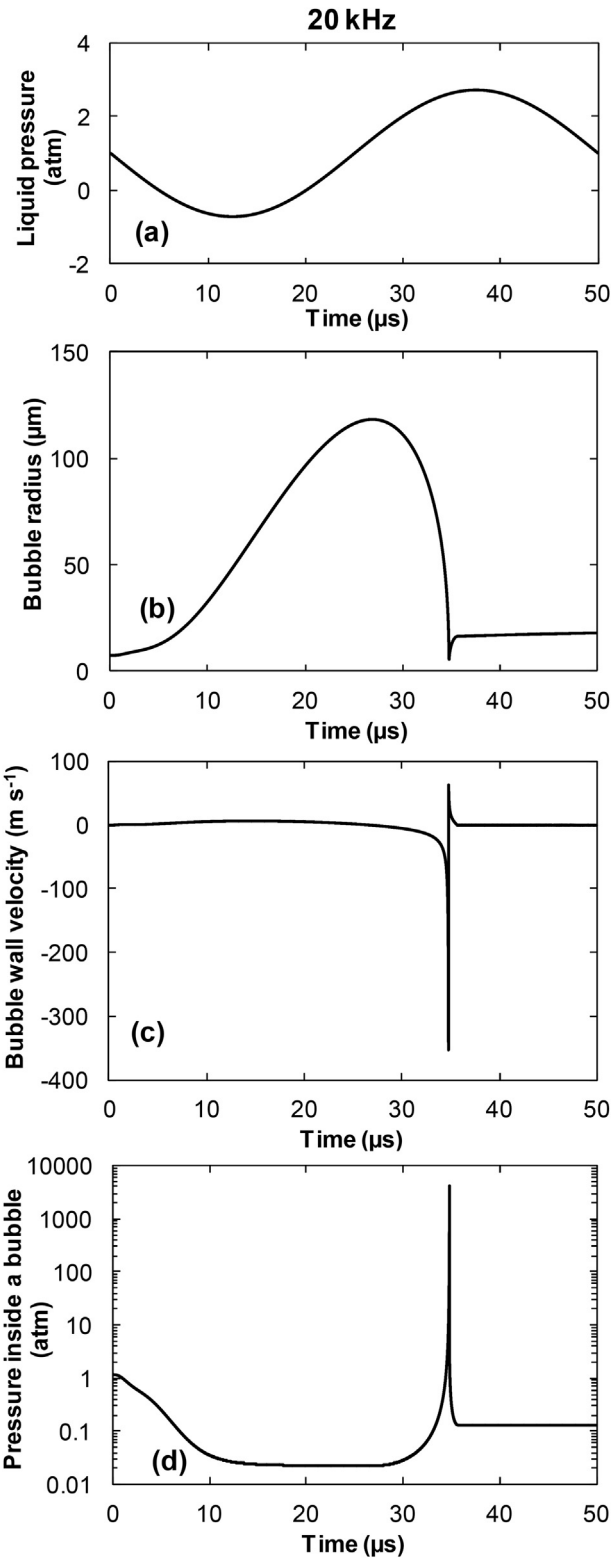

Fig. 2 – The calculated results at 20 kHz as function of time for one acoustic period (50 μs) (conditions: ambient bubble radius: 7.5 μm, acoustic intensity: 1 W cm^{-2}). (a) liquid pressure, (b) bubble radius, (c) bubble wall velocity and (d) pressure inside a bubble. The vertical axis in (d) is in logarithmic scale.

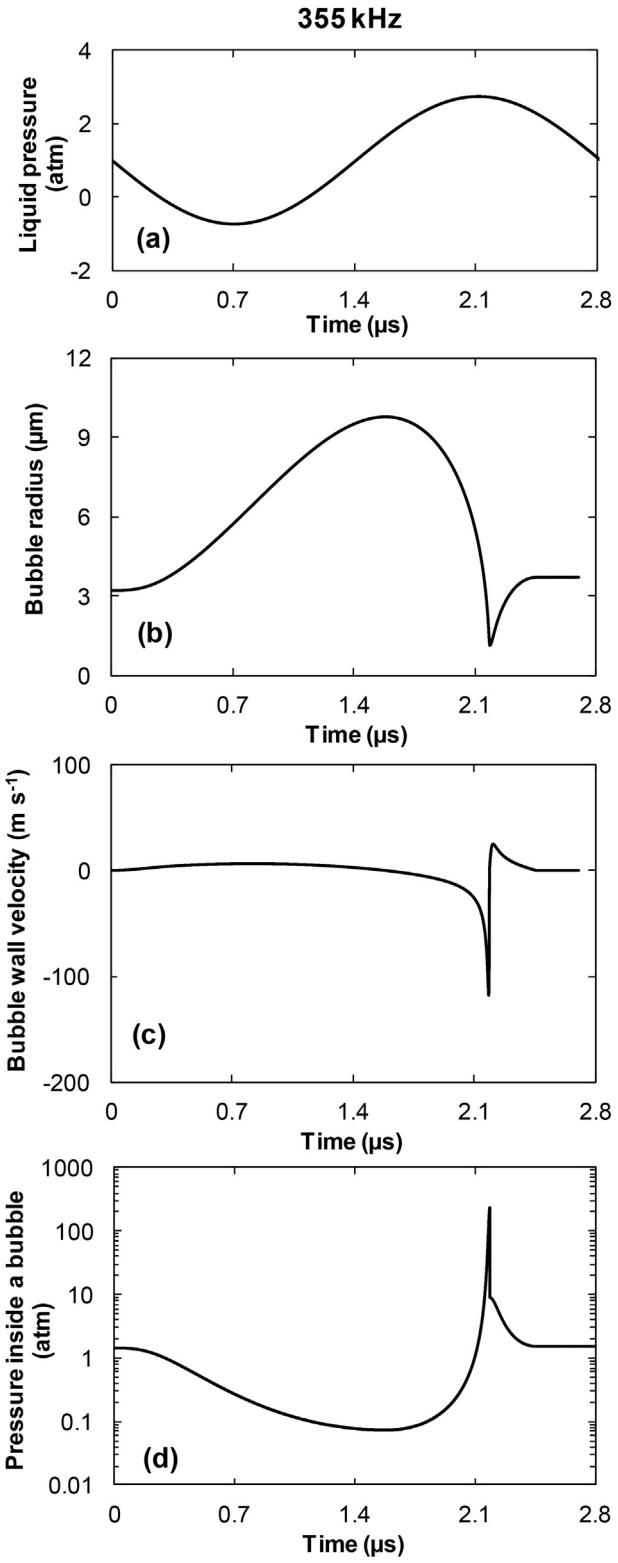

Fig. 3 – The calculated results at 355 kHz as function of time for one acoustic period (2.8 μs) (conditions: ambient bubble radius: 3.2 μm, acoustic intensity: 1 W cm^{-2}). (a) liquid pressure, (b) bubble radius, (c) bubble wall velocity and (d) pressure inside a bubble. The vertical axis in (d) is in logarithmic scale.

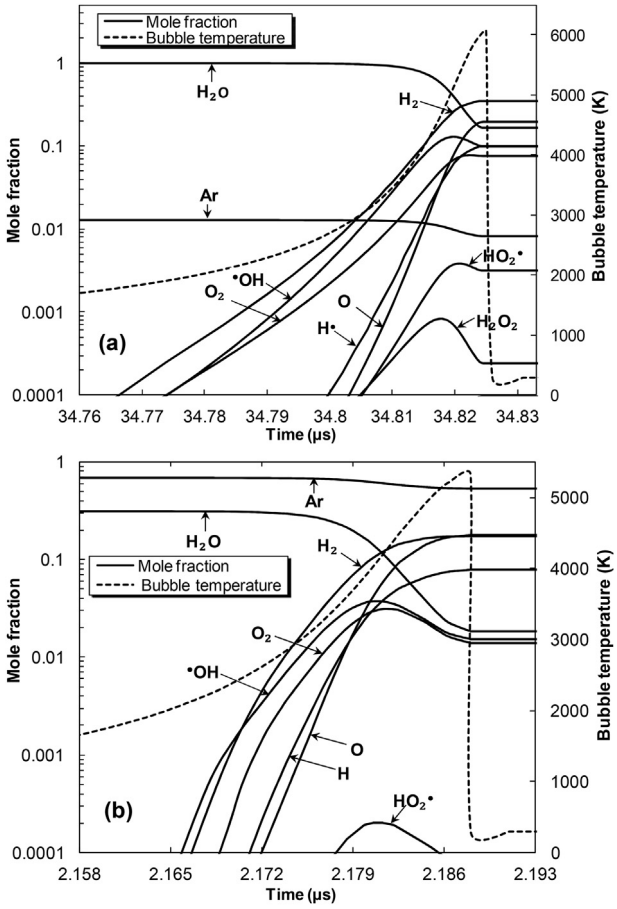

Fig. 4 – Evolution of the reactions system inside a bubble as function of time at around the end of the bubble collapse at (a) 20 kHz and (b) 355 kHz (conditions: ambient bubble radius: 7.5 at 20 kHz and 3.2 μm at 355 kHz, acoustic intensity: 1 W cm^{-2}). The principal vertical axes are in logarithmic scale and the horizontal axes are presented for only ~0.072 μs in (a) and ~0.035 μs in (b).

At 20 kHz, the most initial bubble content is water vapor and trace of argon (Fig. 4(a)). In contrast, at 355 kHz, the bubble is of gaseous nature (Fig. 4(b)). When the temperature and pressure in the bubble increased during the final stage of the bubble collapse, chemical reactions occurred and many chemical products such as H_2, O_2, H_2O_2,•OH, O, H• and HO_2• are created from the thermal dissociation of water vapor and gases molecules and their associate reactions (Fig. 4(a) and (b)). The reaction time is very short (~0.075 μs at 20 kHz and 0.035 μs at 355 kHz). From Fig. 4(a) and (b), it is clearly observed that while •OH and O are the main radical species created, H_2 is the main molecular product formed in the bubble at appreciable amount. Thus, the numerical simulations evidenced the formation of hydrogen during acoustic cavitation event. It was also seen that the H_2 evolution in the bubble attained its upper limit at the end of the bubble collapse (at R_{min}), followed by almost constant production as the bubble temperature decreases suddenly after the end of the bubble collapse. H_2 constitutes more than 35.3% of the bubble contents at 20 kHz and more than 17.2% at 355 kHz. By analyzing the chemical kinetic results, it was found that more than 99%

of H_2 were coming from the reaction $H^\bullet + {}^\bullet OH \leftrightarrow H_2 + O$. Therefore, H_2 was formed in the bubble mainly from the recombination of the primary radicals created in the bubble ($H^\bullet$, $^\bullet OH$). The fort consumption of these radicals at high bubble temperatures is clearly reflected by the appearance of an optimum on the curve of $^\bullet OH$ radical before the end of the bubble collapse, which is the same reason for the higher yield of O atoms at the end of the bubble collapse.

Several authors [32,33] suggested that H_2 is formed mainly through the recombination of hydrogen atoms at the liquid shell of the bubble via the reaction $H^\bullet + H^\bullet \leftrightarrow H_2$. To discuss this suggestion let assuming a number N of active bubbles formed in the cavitating medium (N is of the order of 10^4 *bubbles* L^{-1} s^{-1} at 20 kHz and 10^8 *bubbles* L^{-1} s^{-1} at 355 kHz [34]). Thus, the overall production rates of H_2 (r_{H_2}) can be expressed as

$$r_{H2} = N \times n_{H_2} + k'[^\bullet H]^2 \tag{16}$$

where N (in bubbles L^{-1} s^{-1}) is the number of bubbles collapsing per unit volume per unit time, n_{H_2} (in mol) is the mole number of H_2 released by a single bubble (evaluated at R_{min}) and k' is the liquid rate constant of the reaction $H^\bullet + H^\bullet \leftrightarrow H_2$. The first part of Eq. (16) is related to the production of molecular H_2 from the gas phase of the bubbles through the reaction $H^\bullet + {}^\bullet OH \leftrightarrow H_2 + O$ and the second part is related to the production of H_2 from the reaction $H^\bullet + H^\bullet \leftrightarrow H_2$ at the liquid shell of the bubble. This latter can be related to the production rate of $H^\bullet$ ($r_{H^\cdot}$) as

$$r_{H^\cdot} = N \times n_{H^\cdot} - 2k'[^\bullet H]^2 \tag{17}$$

where $n_{H^\cdot}$ is the mole number of $H^\bullet$ released by a single bubble (evaluated at R_{min}). The steady-state condition for $H^\bullet$ ($r_{H^\cdot} = 0$) gives:

$$k'[^\bullet H]^2 = \frac{1}{2} N \times n_{H^\cdot} \tag{18}$$

By substituting (18) in (16), we obtained:

$$r_{H_2} = N \times n_{H_2} + \frac{1}{2} N \times n_{H^\cdot} \tag{19}$$

Thus, the overall production rate of H_2 shows two routes:

−Production from the gas phase of the bubble, rg : $r_g = N \times n_{H_2}$ (20)

−Production at the liquid shell of the bubble, rl : $r_l = \frac{1}{2} N \times n_{H^\cdot}$ (21)

The ratio of Eq. (20) to Eq. (21) gives:

$$\frac{r_g}{r_l} = 2 \times \frac{n_{H_2}}{n_{H^\cdot}} \tag{22}$$

Expressing n_{H_2} and n_H with the general equation of perfect gases $n_i = y_i \times n_t$, this lead to

$$\frac{r_g}{r_l} = 2 \times \frac{y_{H_2}}{y_{H^\cdot}} \tag{23}$$

where y_{H_2} and $y_{H^\cdot}$ are the mole fractions of H_2 and $H^\bullet$ in the bubble at the final moment of implosion (at R_{min}). They are obtained from Fig. 4(a) and (b) as

- 20 kHz: y_{H_2}=35.3%, $y_{H^\bullet}$=9.78% $\Rightarrow \frac{r_g}{r_l} = 7.22$
- 355 kHz: y_{H_2}=17.2%, $y_{H^\bullet}$=7.86% $\Rightarrow \frac{r_g}{r_l} = 4.37$

Consequently, it can be observed that the production of H_2 from the gas phase of the bubble through the reaction $H^\bullet + {}^\bullet OH \leftrightarrow H_2 + O$ is higher by factors of 7.23 and 4.37, at respectively 20 and 355 kHz, than the production suggested at the liquid shell of the bubble via the reaction $H^\bullet + H^\bullet \leftrightarrow H_2$. The lower r_g/r_l ratio at 355 kHz is well justified by the fact that at high frequency the reaction system inside a bubble has not enough time to evolves and then converts radicals to H_2 through $H^\bullet + {}^\bullet OH \leftrightarrow H_2 + O$ (the reaction time at 20 kHz is ~2 times larger than that at 355 kHz, as indicated in Fig. 4) due to the short bubble collapse time (Figs. 2(b) and 3(b)) at high frequency. Consequently, the formation of H_2 at the shell of the bubble via the reaction $H^\bullet + H^\bullet \leftrightarrow H_2$ is important at 355 kHz than at 20 kHz.

Finally, by regarding the high values of r_g/r_l ratio for both cases (20 and 355 kHz), it can be concluded that the dominant source of H_2 generation during sonolysis of water saturated with argon is the gas phase of the bubble through the reaction $H^\bullet + {}^\bullet OH \leftrightarrow H_2 + O$ whereas the recombination reaction ($H^\bullet + H^\bullet \leftrightarrow H_2$) at the shell of the bubble plays only a minor role.

Conclusions

This study aimed to clarify the mechanism of hydrogen production from water sonolysis. By proposing a mechanism of 25 reversible chemical reactions for the internal bubble-chemistry, a series of numerical simulations of chemical reactions occurring in a bubble oscillating in liquid water irradiated by an ultrasonic wave have been performed for various conditions. On the basis of the simulation results, material balance for hydrogen production in the gas and liquid phases has been carried out to evaluate the internal-bubble and the external-bubble ways of H_2 production. The numerical simulations have evidenced the formation of H_2 in the bubble. By analyzing the results of the predicted production rate of H_2 in the gas and liquid phases, it was concluded that the main source of H_2 production during water sonolysis is the gas phase of the bubbles through the reaction $H^\bullet + {}^\bullet OH \leftrightarrow H_2 + O$.

Acknowledgments

The financial support by the Ministry of Higher Education and Scientific Research of Algeria (project No. J0101120120098) is greatly acknowledged.

REFERENCES

[1] Haryanto A, Fernando S, Murali N, Adhikari S. Current status of hydrogen production techniques by steam reforming of ethanol: a review. Energy Fuels 2005;19:2098–106.

[2] Yavor Y, Goroshin S, Bergthorson JM, Frost DL. Comparative reactivity of industrial metal powders with water for

hydrogen production. Int J Hydrogen Energy 2015;40:1026–36.
[3] Marbán G, Valdés-Solís T. Towards the hydrogen economy. Int J Hydrogen Energy 2007;32:1625–37.
[4] Santos DMF, Sequeira CAC, Figueiredo JL. Hydrogen production by alkaline water electrolysis. Quim Nova 2013;36:1176–93.
[5] Marino F, Boveri M, Baronetti G, Laborde M. Hydrogen production via catalytic gasification of ethanol. A mechanism proposal over copper–nickel catalysts. Int J Hydrogen Energy 2004;29:67–71.
[6] Onda K, Kyakuno T, Hattori K, Ito K. Prediction of production power for high-pressure hydrogen by high-pressure water electrolysis. J Power Sources 2004;132:64–70.
[7] Das D, Veziroglu TN. Hydrogen production by biological processes: a survey of literature. Int J Hydrogen Energy 2001;26:13–28.
[8] He D, Bultel Y, Magnin J-P, Willison J-C. Kinetic analysis of photosynthetic growth and photohydrogen production of two strains of *Rhodobacter capsulatus*. Enzyme Microb Technol 2006;38:253–9.
[9] Rosseler O, Shankar MV, Karkmaz-Le DM, Schmidlin L, Keller N, Keller V. Solar light photocatalytic hydrogen production from water over Pt and Au/TiO (anatase/rutile) photocatalysts: influence of noble metal and porogen promotion. J Catal 2010;269:179–90.
[10] Rodriguez J, Thivel PX, Puzenat E. Photocatalytic hydrogen production for PEMFC supply: a new issue. Int J Hydrogen Energy 2013;38:6344–8.
[11] Molinari R, Marino T, Argurio P. Photocatalytic membrane reactors for hydrogen production from water. Int J Hydrogen Energy 2014;39:7247–61.
[12] Harada H. Isolation of hydrogen from water/or artificial seawater by sonophotocatalysis using alternating irradiation method. Int J Hydrogen Energy 2011;26:303–7.
[13] Fischer CH, Hart EJ, Henglein A. H/D exchange in the D_2–H_2O system under the influence of ultrasound. J Phys Chem 1986;90:222–4.
[14] Hart EJ, Fischer CH, Henglein A. Isotopic exchange in the sonolysis of aqueous solutions containing $^{14.14}N_2$ and $^{15.15}N_2$. J Phys Chem 1986;90:5989–91.
[15] Yang Y, Gai WZ, Deng ZY, Zhou JG. Hydrogen generation by the reaction of Al with water promoted by an ultrasonically prepared $Al(OH)_3$ suspension. Int J Hydrogen Energy 2014;39:18734–42.
[16] Gentili PL, Penconi M, Ortica F, Cotana F, Rossi F, Elisei F. Synergistic effects in hydrogen production through water sonophotolysis catalyzed by new $La_{2x}Ga_{2y}In_{2(1-x-y)}O_3$ solid solutions. Int J Hydrogen Energy 2009;34:9042–9.
[17] Dharmarathne L, Ashokkumar M, Grieser F. Photocatalytic generation of hydrogen using sonoluminescence and sonochemiluminescence. J Phys Chem C 2012;116:1056–60.
[18] Cotana F, Rossi F, Urbani M. Study of water photosonolysis for hydrogen production. In: 3rd International green energy conference; 2007. Västerås, Sweden.
[19] Guo Y, Kim S, Sung S, Lee P. Effect of ultrasonic treatment of digestion sludge on bio-hydrogen production from sucrose by anaerobic fermentation. Int J Hydrogen Energy 2010;35:3450–5.
[20] Leano EP, Anceno AJ, Babel S. Ultrasonic pretreatment of palm oil mill effluent: impact on biohydrogen production, bioelectricity generation, and underlying microbial communities. Int J Hydrogen Energy 2012;37:12241–9.
[21] Elbeshbishy E, Hafez H, Nakhla G. Hydrogen production using sono-biohydrogenator. Int J Hydrogen Energy 2011;36:1456–65.
[22] Gadhe A, Sonawane SS, Varma MN. Evaluation of ultrasonication as a treatment strategy for enhancement of biohydrogen production from complex distillery wastewater and process optimization. Int J Hydrogen Energy 2014;39:10041–50.
[23] Pétrier C. The use of power ultrasound for water treatment. In: Gallego-Juarez JA, Graff KF, editors. Power ultrasonics: applications of high-intensity ultrasound. Cambridge: Elsevier; 2015. p. 939–63.
[24] Venault L. De l'influence des ultrasons sur la réactivité de l'uranium (U(IV)/U(VI)) et du plutonium (PU(III)/PU(IV)) en solution aqueuse nitrique [Thèse de Doctorat]. Université de Paris XI Orsay; 1997.
[25] Suslick KS, Didenko Y, Fang MM, Hyeon T, Kolbeck KJ, McNamara WB, et al. Acoustic cavitation and its chemical consequences. Phil Trans Roy Soc A – Math Phys Eng Sci 1999;357:335–53.
[26] Leighton TG. The acoustic bubble. London: Academic Press; 1994.
[27] Suslick KS, Flannigan DJ. Inside a collapsing bubble: sonoluminescence and the conditions during cavitation. Annu Rev Phys Chem 2008;59:659–83.
[28] Hart EJ, Henglein A. Sonochemistry of aqueous solutions: H_2–O_2 combustion in cavitation bubbles. J Phys Chem 1987;91:3654–6.
[29] Adewuyi YG. Sonochemistry: environmental science and engineering applications. Ind Eng Chem Res 2001;40:4681–715.
[30] Anbar M, Pecht I. On the sonochemical formation of hydrogen peroxide in water. J Phys Chem 1964;68:352–5.
[31] Anbar M, Pecht I. The sonolytic decomposition of organic solutes in dilute aqueous solutions. I. Hydrogen abstraction from sodium formate. J Phys Chem 1964;68:1460–2.
[32] Fischer CH, Hart EJ, Henglein A. Ultrasonic irradiation of water in the presence of $^{18.18}O_2$: isotope exchange and isotopic distribution of H_2O_2. J Phys Chem 1986;90:1954–6.
[33] Gutihez M, Henglein A, Dohrmann JK. H atom reactions in the sonolysis of aqueous solutions. J Phys Chem 1987;91:6687–90.
[34] Merouani S, Hamdaoui O, Rezgui Y, Guemini M. A method for predicting the number of active bubbles in sonochemical reactors. Ultrason Sonochem 2015;22:51–8.
[35] Merouani S, Hamdaoui O, Rezgui Y, Guemini M. Theoretical estimation of the temperature and pressure within collapsing acoustical bubbles. Ultrason Sonochem 2014;21:53–9.
[36] Merouani S, Hamdaoui O, Rezgui Y, Guemini M. Theoretical procedure for the characterization of acoustic cavitation bubbles. Acta Acust United Acust 2014;100:823–33.
[37] Crum LA. The polytrophic exponent of gas contained within air bubbles pulsating in a liquid. J Acoust Soc Am 1983;73:116–20.
[38] Keller JB, Kolodner II. Damping of underwater explosion bubble oscillations. J Appl Phys 1956;27:1152–61.
[39] Keller JB, Miksis MJ. Bubble oscillations of large amplitude. J Acoust Soc Am 1980;68:628–33.
[40] Colussi AJ, Weavers LK, Hoffmann MR. Chemical bubble dynamics and quantitative sonochemistry. J Phys Chem A 1998;102:6927–34.
[41] Yasui K. Effect of non-equilibrium evaporation and condensation on bubble dynamics near the sonoluminescence threshold. Ultrasonics 1998;36:575–80.
[42] Storey BD, Szeri AJ. Water vapor, sonoluminescence and sonochemistry. Proc R Soc Lond A 2000;456:1685–709.
[43] Kamath V, Prosperetti A, Egolfopoulos FN. A theoretical study of sonoluminescence. J Acoust Soc Am 1993;94:248–60.

[44] Fujikawa S, Akamatsu T. Effects of the non-equilibrium condensation of vapour on the pressure wave produced by the collapse of a bubble in a liquid. J Fluid Mech 1980;97:481–512.
[45] Conaire MO, Curran HJ, Simmie JM, Pitz WJ, Westbrook CK. A comprehensive modeling study of hydrogen oxidation. Int J Chem Kinet 2004;36:603–22.
[46] Mueller MA, Kim TJ, Yetter RA, Dryer FL. Flow reactor studies and kinetic modeling of the H_2/O_2 reaction. Int J Chem Kinet 1999;31:113–25.
[47] Kanthale P, Ashokkumar F, Grieser F. Sonoluminescence, sonochemistry (H_2O_2 yield) and bubble dynamics: frequency and power effects. Ultrason Sonochem 2008;15:143–50.
[48] Jiang Y, Petrier C, Waite TD. Sonolysis of 4-chlorophenol in aqueous solution: effects of substrate concentration, aqueous temperature and ultrasonic frequency. Ultrason Sonochem 2006;13:415–22.
[49] Koda S, Kimura T, Kondo T, Mitome H. A standard method to calibrate sonochemical efficiency of an individual reaction system. Ultrason Sonochem 2003;10:149–56.
[50] Beckett MA, Hua I. Impact of ultrasonic frequency on aqueous sonoluminescence and sonochemistry. J Phys Chem A 2001;105:3796–802.
[51] Burdin F, Tsochatzidis NA, Guiraud P, Wilhelm AM, Delmas H. Characterisation of the acoustic cavitation cloud by two laser techniques. Ultrason Sonochem 1999;6:43–51.
[52] Tsochatzidis NA, Guiraud P, Wilhelm A, Delmas H. Determination of velocity, size and concentration of ultrasonic cavitation bubbles by the phase-doppler technique. Chem Eng Sci 2001;56:1831–40.
[53] Brotchie A, Grieser F, Ashokkumar M. Effect of power and frequency on bubble-size distributions in acoustic cavitation. Phys Rev Lett 2009;102. 084302-1–4.

Nomenclature and units

c: speed of sound in the liquid medium, m s^{-1}
f: frequency of ultrasonic wave, Hz
I_a: acoustic intensity of ultrasonic irradiation, W m^{-2}
p: pressure inside a bubble, Pa
p_{max}: maximum pressure inside a bubble, Pa
p_∞: ambient static pressure, Pa
P_A: amplitude of the acoustic pressure, Pa
P_v: vapor pressure of water, Pa
P_{g0}: initial gas pressure, Pa
R: radius of the bubble, m
R_{max}: maximum radius of the bubble, m
R_0: ambient bubble radius, m
t: time, s
T: temperature inside a bubble, K
T_{max}: maximum temperature inside a bubble, K
T_∞: bulk liquid temperature, K

Greek letters

γ: specific heat ratio (c_p/c_v) of the gas mixture
σ: surface tension of liquid water, N m^{-1}
ρ: density of liquid water, kg m^{-3}